JOURNAL OF MATERIALS SCIENCE **35** (2000) 3827–3835

Effect of $MoSi_2$ and Nb reinforcements on mechanical properties of Al_2O_3 matrix composites

A. CHAKRABORTY, S. V. KAMAT, R. MITRA
Defence Metallurgical Research Laboratory, Hyderabad - 500058, India
E-mail: amitav@dmrl.ernet.in

K. K. RAY
Indian Institute of Technology, Kharagpur - 721302, India

The room temperature mechanical properties of Al_2O_3 composites reinforced with 25 vol% of either $MoSi_2$ or Nb particulates were investigated. It was found that addition of Nb particles resulted in a reduction in the elastic modulus, but caused a significant increase in both flexural strength and fracture toughness. On the other hand, the addition of $MoSi_2$ particles resulted in only a marginal decrease in elastic modulus and marginal increase in both flexural strength and fracture toughness. The elastic modulus results were explained on the basis of Tsai - Halpin model. For both the composites, the increase in flexural strength was attributed to the grain refinement of the Al_2O_3 matrix as well as the load transfer to the reinforcement particles. The marginal increase in fracture toughness in Al_2O_3 / $MoSi_2$ composites was attributed to crack deflection, whereas the threefold increase in fracture toughness in Al_2O_3 / Nb composites was attributed to crack blunting and bridging.

1. Introduction

There has recently been a resurgence of interest in ceramics for a variety of high performance structural applications, ranging from high temperature gas turbines and adiabatic diesel engines to cutting tools and other wear-resistant parts [1]. In each case the applications make use of the beneficial properties of ceramics, including high stiffness, strength and hardness, low density and good resistance to corrosion, oxidation, wear and erosion at high temperatures. In most structural applications, the primary disadvantage of ceramics is their inherent lack of toughness, which renders them sensitive to sudden catastrophic failure in response to accidental overloading, contact damage or rapid temperature changes. This has led to attempts for developing ceramic composites which provide the best possible toughness and thermal shock resistance without significant loss of other desirable properties [2].

A variety of stratagems has been adopted in the search for greater toughness. These include incorporation of metallic and/or ceramic fibers and/or whiskers [2–5]; incorporation of more or less equiaxed second-phase particles, both ductile [6–9] and brittle [10, 11]; control of grain size, porosity or other microstructural features [12, 13]; and transformation toughening by the incorporation of tetragonal ZrO_2 particles [14, 15]. Second phase particles can play a number of roles. They can deflect cracks out of their paths [16, 17], can bridge the crack behind the crack tip [18], cause them to bow between obstacles [19], cause them to bifurcate [20], or cause the nucleation of additional microcracks ahead of the primary crack [21].

2. Present study

The present work is concerned with establishing the room temperature mechanical properties of Al_2O_3 matrix composite systems incorporated with two different reinforcements: i) Molybdenum Disilicide ($MoSi_2$) & ii) Niobium (Nb).

Although $MoSi_2$ has recently been investigated as a matrix material for high temperature structural composites [22, 23], it is also considered to be as a potential reinforcement for different ceramic matrices [24, 25]. Nb, as a refractory metal, is also being considered as a capable toughening element for brittle ceramic matrices [26]. Although extensive studies have been carried out by a number of investigators on Al_2O_3 based composites incorporated with different ceramic reinforcements, no such research results are available in literature in regards to the properties of either Al_2O_3 - Nb or Al_2O_3 - $MoSi_2$ composite. It is known that unlike other ceramic reinforcements (e.g. SiC, TiC, TiB_2, B_4C, etc.) the thermal expansion coefficient values of both $MoSi_2$ and Nb are much closer to that of Al_2O_3 (Fig. 1) [27]. As a result, the residual stress originating from the thermal expansion coefficient mismatch (between matrix and reinforcement) would be minimum for both these composites, which might act as a beneficial parameter for the materials. Secondly, it has also been demonstrated earlier that both Nb and $MoSi_2$ are chemically compatible with Al_2O_3 and as a result, reaction free clean interfaces between matrix and reinforcement can be achieved by careful processing in both the cases, which is a desirable criterion from mechanical properties point of view [27, 28].

TABLE I Source and average particle size of the as received raw materials

Sl. No.	Material	Source	Average Particle size (μm)
1	Al_2O_3	M/s Baikowski International, USA	0.40 (after milling)
2	$MoSi_2$	M/s H. G. Starck, Germany	5.85
3	Nb	M/s New Metals Co., UK	10.01

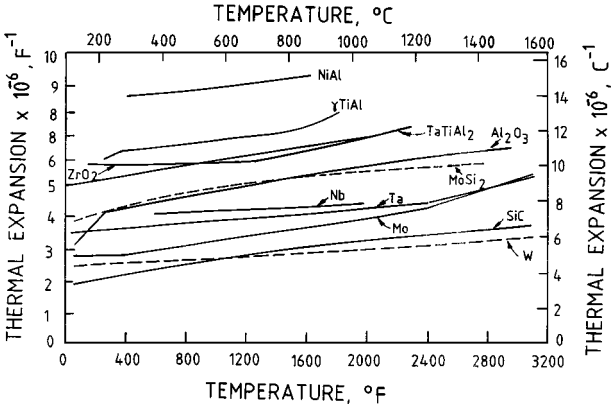

Figure 1 Comparative thermal expansion co-efficients of Al_2O_3, $MoSi_2$ & Nb.

3. Experimental

High purity Al_2O_3, $MoSi_2$ and Nb powders were used in the present study. The particle size analysis data obtained for all the three materials (using a Microanalyzer, Japan make instrument based on sedimentation technique) are shown in Fig. 2. Table I shows the source and average particle size of the as-received raw materials. The process flow chart followed for making these composites (Al_2O_3 / 25 vol% $MoSi_{2p}$ and Al_2O_3 / 25 vol% Nb_p) is illustrated in Fig. 3. Al_2O_3 and $MoSi_2$ or Nb powders were taken in the required proportions and then wet blended in an ultrasonic mixer. The blended powder was vacuum hot pressed using a GCA, USA make hot press at temperatures between 1550°C and 1650°C and pressure of 30 MPa. For the sake of comparison, pure Al_2O_3 without any reinforcement was also processed following the pressureless sintering route.

The hot pressed discs were characterized by evaluating their respective bulk densities using Archimedes Principle. The % T.D. values obtained for all the materials are given in Table II. The distribution of second phase reinforcement in the matrix was observed by scanning electron microscopy. Electron Probe Microanalysis (EPMA) studies were also carried out to establish the chemical stability of all the phases. Transmission Electron Microscopy (TEM) was also carried out for both the composites in order to study the interface between the matrix and reinforcement. The elastic modulus values for the monolithic matrix and the composites were determined using a pulse - echo overlap technique [29] and those data are given in Table II. Flexural strength was measured on a Instron 1185 Testing machine using 3 point bend specimens. A loading

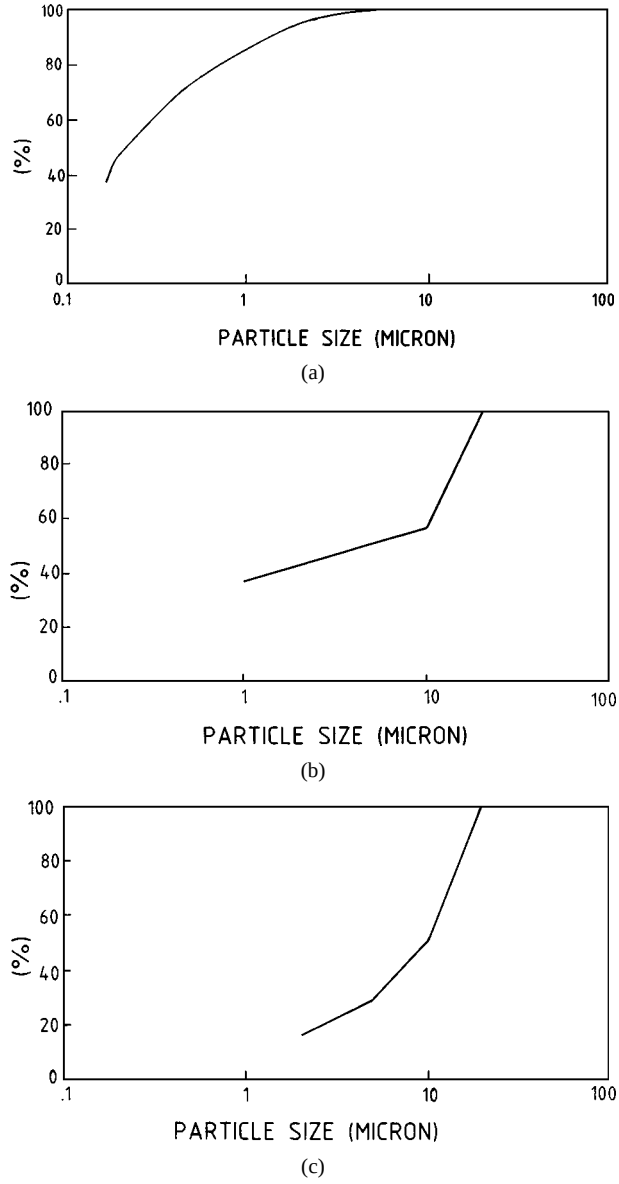

Figure 2 Particle size analysis data for : (a) Al_2O_3, (b) $MoSi_2$ & (c) Nb powders.

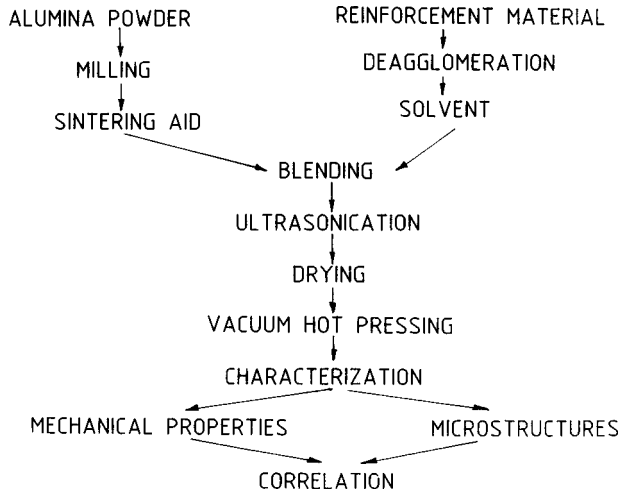

Figure 3 Process flow chart followed for fabricating the composites.

rate of 0.5 mm / min was used during testing of all the samples. The test samples were prepared in the form of rectangular bar specimens having dimensions as: 40 mm (Span : L) × 5 mm (Breadth : B) × 5 mm

TABLE II Properties of the matrix and composite materials

Properties / Material	% T. D.	Hardness (GPa)	Fracture Toughness (MPa$\sqrt{m}$)	Flexural Strength (MPa)	Elastic Modulus (GPa)
Al_2O_3	98.6	15.8	3.6	275	390
$Al_2O_3 + 25$ vol% Nb	98.1	13.2	10.1	580	304
$Al_2O_3 + 25$ vol% $MoSi_2$	98.2	13.5	4.2	360	385

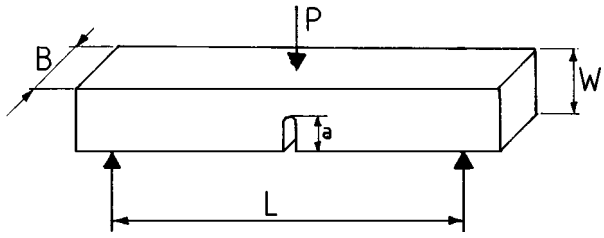

Figure 4 Schematic diagram for the SENB fracture toughness test sample.

(Width : W). The flexural strength, σ, was calculated as, $\sigma = 3P_{\max}L\ /\ 2BW^2$, where, $P_{\max}$ is the maximum load obtained from the load displacement curve. Fracture toughness (K_{IC}) was determined using single edge notched beam (SENB) specimen (under 3 point bend loading) having following dimensions : Span (L) = 40 mm, Breadth (B) = 5 mm and Width (W) = 10 mm. The notch in the SENB specimen was made using a ISOMET diamond wheel having a thickness of $\sim$100 μm which resulted in a notch root radius of $\sim$60 μm. The notch depth was maintained at about 0.5 to 0.55 W (Fig. 4). The fracture toughness values were calculated using the following equation [30],

$$K_{IC} = \left(\frac{PL}{BW^{3/2}}\right) f\left(\frac{a}{W}\right),$$

with,

$$f\left(\frac{a}{W}\right) = 3\left(\frac{a}{W}\right)^{1/2}\left[1.99 - \left(\frac{a}{W}\right)\left\{1 - \left(\frac{a}{W}\right)\right\} \times \left\{2.15 - 3.93\left(\frac{a}{W}\right) + 2.7\left(\frac{a}{W}\right)^2\right\}\right] \times \left[2\left\{1 + 2\left(\frac{a}{W}\right)\right\}\left\{1 - \left(\frac{a}{W}\right)\right\}^{3/2}\right]^{-1},$$

"a" and "P" being the respective notch tip radius and the max. load obtained from the load displacement curve

The fractured specimens were examined using both JEOL and LEO scanning electron microscopes. Indentation tests were also carried out for studying the crack path - microstructure interactions.

4. Results

Fig. 5a and b show the respective SEM pictures of as received $MoSi_2$ and Nb powders. It is observed that both $MoSi_2$ and Nb particles are equiaxed in nature. The scanning electron micrographs for polished Al_2O_3 (matrix), $Al_2O_3 + MoSi_2$ (AM) and $Al_2O_3 + Nb$ (AN) composites are shown in Fig. 6a–c, respectively. Fig. 6b and c show that both the composites have an uniform distribution of equiaxed reinforcement particles in the matrix. There is also very little evidence of porosity which is reflected in the high % theoretical density achieved for all the three materials (see Table II).

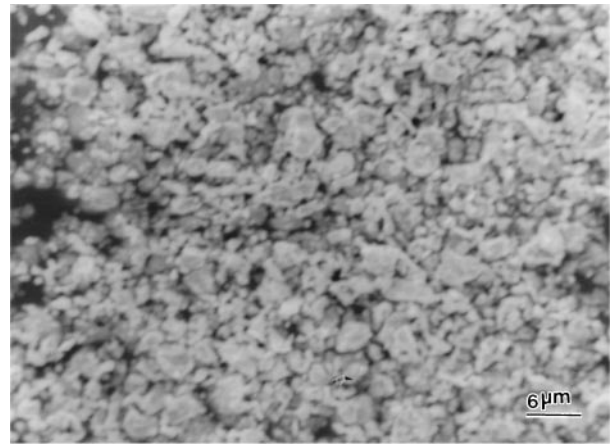

(a)

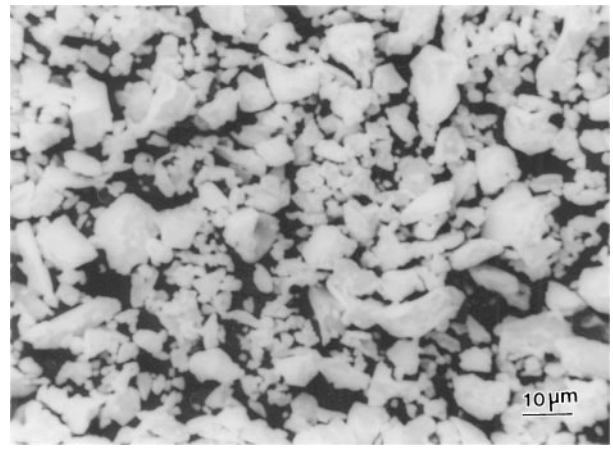

(b)

Figure 5 SEM pictures of the as received : (a) $MoSi_2$ & (b) Nb powders.

Figs 7 and 8 show the back scattered image as well as the relevant elemental maps obtained from EPMA for AM and AN composites, respectively. These figures show that both $MoSi_2$ and Nb have retained their chemical identity in the composite after processing. The prevention of oxidation during processing could be attributed to the high level of vacuum (10^{-5} torr) used during the hot pressing operation. The TEM micrographs of the interface region in both the composites are shown in Fig. 9. A clean reaction free interface is seen in both composites.

The values of the elastic modulus for Al_2O_3 as well as the two composites are given in Table II. It is seen from this Table that AN composite has a significantly lower elastic modulus than that of monolithic Al_2O_3, whereas AM composite has a marginally lower elastic modulus than that of the Al_2O_3 matrix. The flexural strength data is also given in Table II. It is noticed from this Table that both composites exhibit a significantly higher strength than that exhibited by the unreinforced

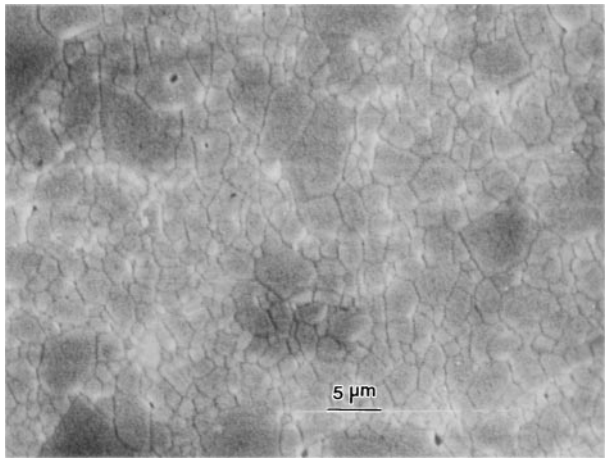

(a)

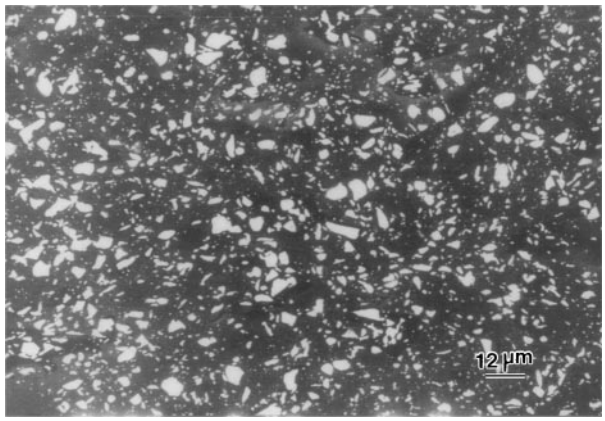

(b)

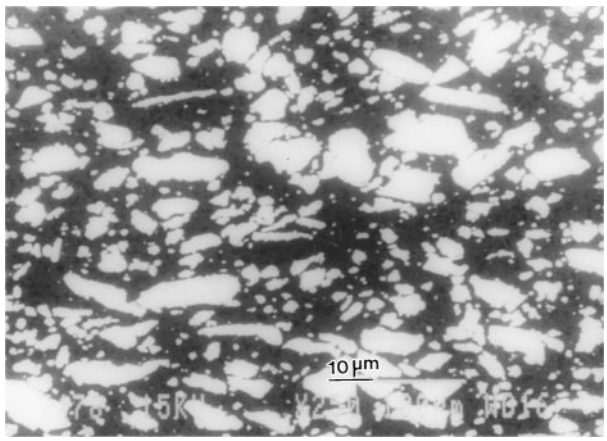

(c)

Figure 6 SEM pictures of polished : (a) Al_2O_3, (b) Al_2O_3 - $MoSi_2$ & (c) Al_2O_3 - Nb samples.

Al_2O_3. The respective flexural strengths of the AM and AN composites are about 30% and 110% higher than that of monolithic Al_2O_3 matrix.

The fracture toughness data is also given in Table II. It shows that AM composite exhibits a marginally higher fracture toughness than that exhibited by the unreinforced Al_2O_3, whereas AN composite shows a significantly higher fracture toughness (three fold increase) than that exhibited by Al_2O_3.

SEM fractographs of the fractured surfaces for Al_2O_3, AM composite and AN composite are shown in Fig. 10. The fracture is intergranular in nature in the case of unreinforced Al_2O_3 (Fig. 10a), whereas both intergranular and transgranular features are seen in case of the composites (Fig. 10b and c). There is very little evidence of pull out of the reinforcement particles in both the composites. However, some fractured $MoSi_2$ particles (Fig. 10d) and a few fractured / deformed Nb particles (Fig. 10c) are observed on the respective fractured surfaces. The fractographs also show that there is considerable refinement in the Al_2O_3 grain size (Fig. 10b : matrix grain size $\approx$ 2.7 μm in Al_2O_3 - $MoSi_2$ and Fig. 10e : matrix grain size $\approx$ 2.8 μm in Al_2O_3 - Nb composite) in the composites as compared to that in the unreinforced Al_2O_3 (Fig. 10a : grain size $\approx$ 4 μm).

The SEM micrographs showing the paths of the cracks emanating from corners of indentations in monolithic Al_2O_3, AM composite and AN composite are shown in Fig. 11. Fig. 11a shows that the crack path in unreinforced Al_2O_3 is nominally straight and there is very little evidence of crack deflection. Fig. 11b shows that in the case of AM composite there is evidence of both microscopic crack deflection as well as crack bridging. On the other hand, the primary feature in AN composite is crack blunting (Fig. 11c) and bridging by the Nb particles (Fig. 11d), although there is some evidence of microscopic crack deflection (Fig. 11d). The frequency versus angle of deflection plot for all the three materials is shown in Fig. 12. It can be seen that AM composite has the highest median angle of deflection.

5. Discussion

5.1. Elastic modulus

There are several theoretical models for the estimation of elastic modulus of composite materials such as the iso - strain and iso - stress rule of mixtures [31], modified Tsai - Halpin [32] and Hashin - Shtrikman [33]. The iso - strain and iso - stress rule of mixtures are most suitable for continuous fibre reinforced composites for loading in the direction of the fibres and perpendicular to the direction of the fibres, respectively. For composites with discontinuous particulate reinforcements, models such as the modified Tsai - Halpin [31] which takes into account the tensile transfer of loads at the particle ends as well as the particle aspect ratio are more appropriate. This model predicts the elastic modulus of the composite (E_c) as,

$$E_c = \frac{\{E_m(1 + 2sqV_p)\}}{(1 - qV_p)} \quad (1)$$

with

$$q = \frac{\left\{\left(\frac{E_p}{E_m}\right) - 1\right\}}{\left\{\left(\frac{E_p}{E_m}\right) + 2s\right\}},$$

where, E_m and E_p are the elastic modulus of the matrix and reinforcement, respectively; s is the aspect ratio of the particle reinforcement; V_p is the volume fraction of the reinforcement. It is known from literature that $E_{Nb} = 103$ GPa [34] and $E_{MoSi2} = 400$ GPa [35], whereas E_{Al2O3} was measured to be 390 GPa. For both

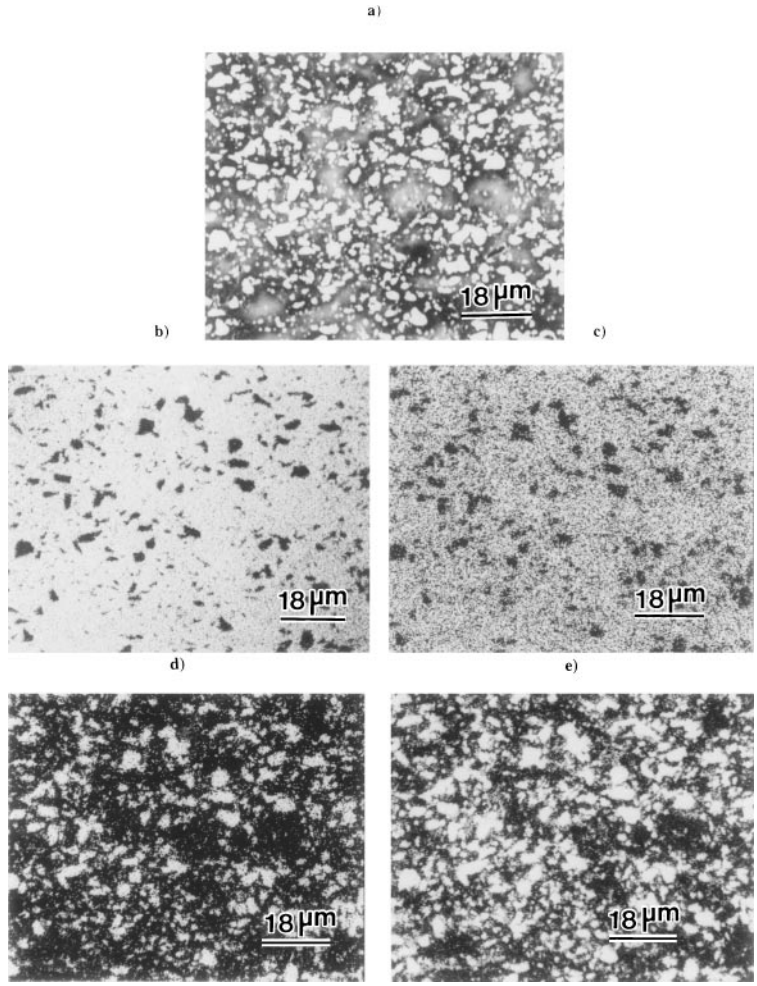

Figure 7 EPMA images of Al_2O_3 - $MoSi_2$ composite showing : (a) backscattered electron image; x-ray elemental maps of : (b) Al, (c) O, (d) Mo & (e) Si.

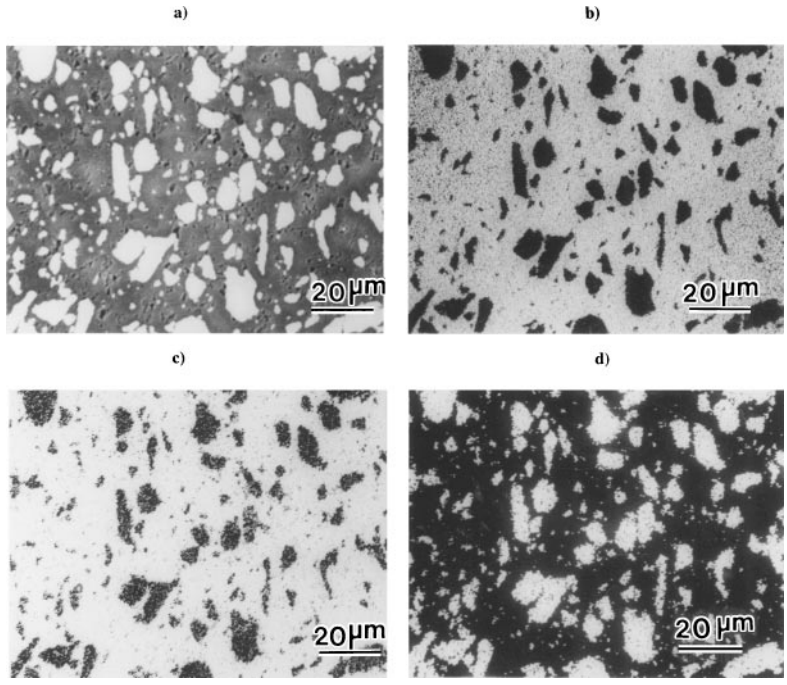

Figure 8 EPMA images of Al_2O_3 - Nb composite showing : (a) backscattered electron image; x-ray elemental maps of : (b) Al, (c) O & (d) Nb.

composites, $V_p = 0.25$ and the aspect ratio is ≈ 1 (for equiaxed particles). Using the above values, Equation 1 predicts a value of 302 GPa for AN composite and 392 GPa for AM composite, which agree very well with the experimentally determined values.

5.2. Flexural strength

As discussed earlier, the flexural strength of AM and AN composites are about 30% and 110% higher than the strength of monolithic Al_2O_3 matrix, respectively. The higher strength of the composites can be attributed

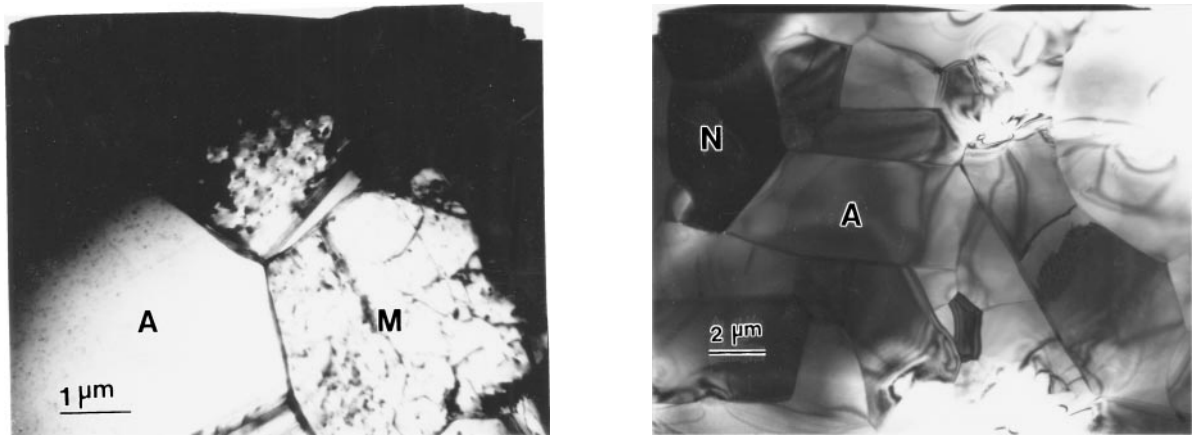

(a) (b)

Figure 9 TEM pictures showing clean interface between : (a) Al_2O_3 and $MoSi_2$ & (b) Al_2O_3 and Nb; (A : Al_2O_3, M : $MoSi_2$ & N : Nb).

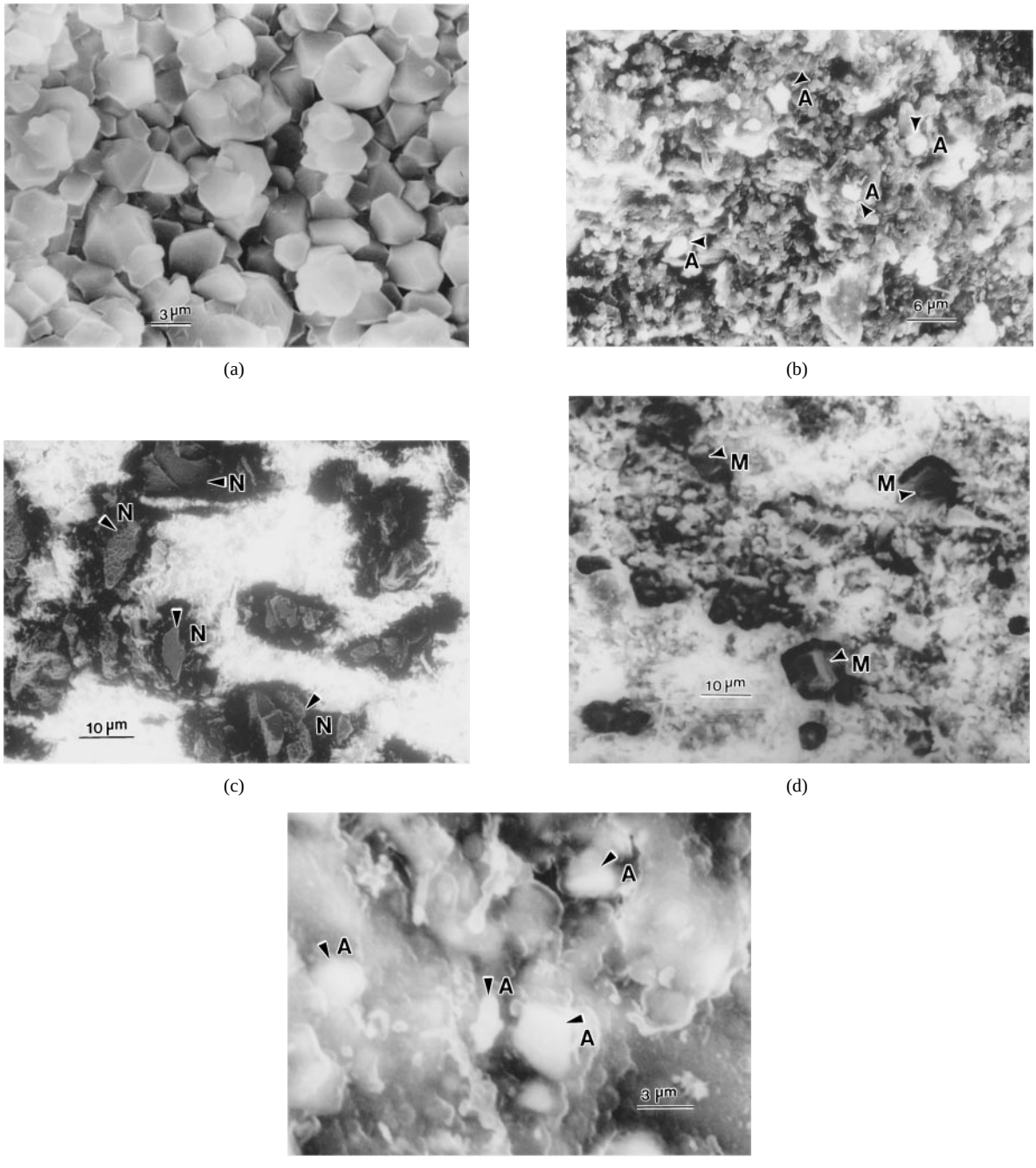

(a) (b)

(c) (d)

(e)

Figure 10 SEM fractographs of the fractured surfaces of : (a) Al_2O_3, (b) Al_2O_3 - $MoSi_2$, (c) Al_2O_3 - Nb, (d) Al_2O_3 - $MoSi_2$ & (e) Al_2O_3 - Nb composites; (A : Al_2O_3, M : $MoSi_2$ & N : Nb).

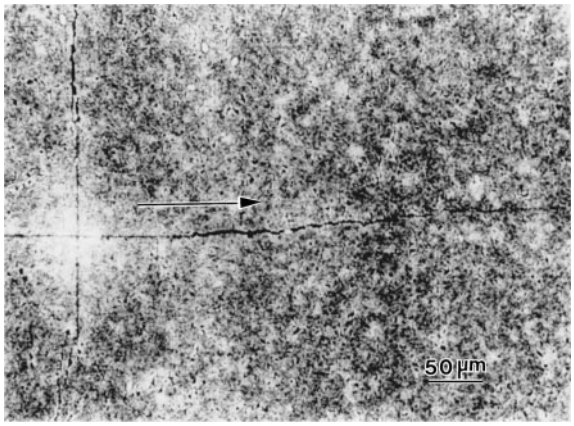

(a)

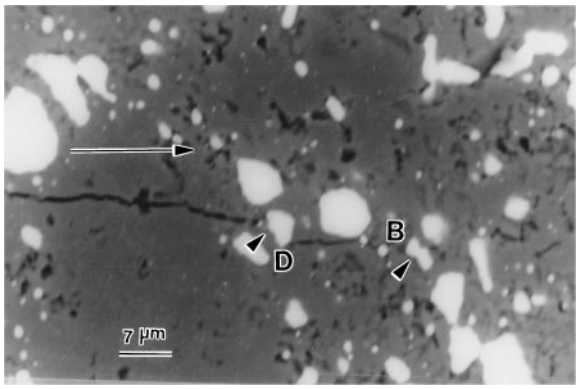

(b)

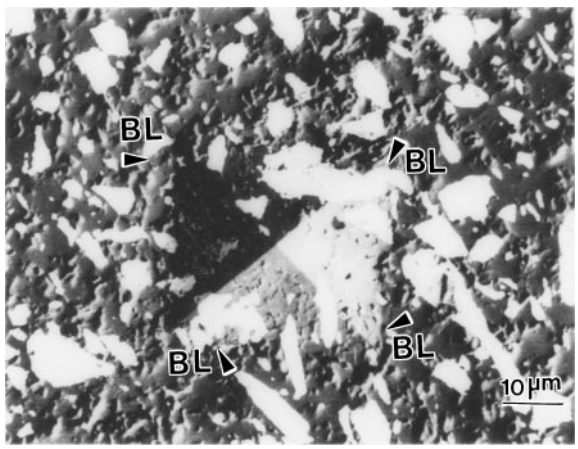

(c)

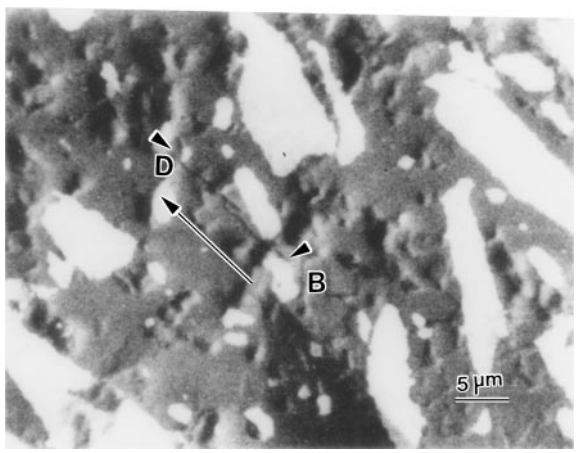

(d)

Figure 11 SEM pictures showing the crack path behaviour in : (a) Al_2O_3, (b) Al_2O_3 - $MoSi_2$, (c) Al_2O_3 - Nb & (d) Al_2O_3 - Nb samples; (D : Deflection, B : Bridging & BL : Blunting) : Long arrow shows direction of crack propagation in all materials.

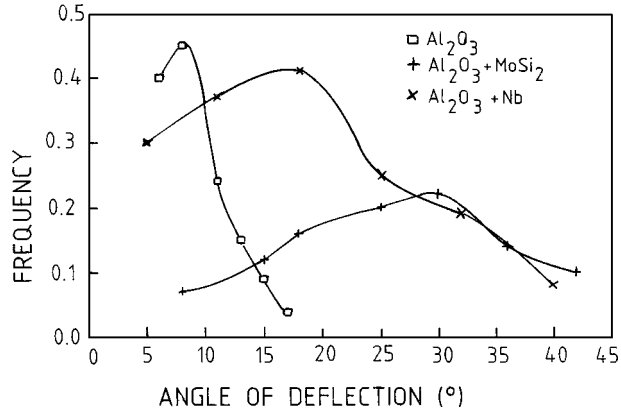

Figure 12 Frequency vs. Deflection angle data for the matrix and the composites.

to the following factors. The first is that the presence of the reinforcement particles results in the refinement in the grain size of the Al_2O_3 matrix in the composites (see Fig. 10a, b and e). The average grain size of unreinforced Al_2O_3 is $\approx$4 μm, whereas it is about 2.7 μm and 2.8 μm for AM and AN composites respectively. The second factor which could contribute to the strengthening is the load transfer to the reinforcement phase which is comparatively stronger than the matrix. The load transfer is efficient in these composites because the interfaces are observed to be clean for both the materials (as seen in Fig. 9a and b). The efficient load transfer is also confirmed by the evidence of very little pull out of the reinforcement particles on the respective fractured surfaces (Fig. 10b–e).

The strengthening behaviour due to matrix grain size refinement should be more or less equal for both the composites. However, the strengthening due to load transfer would be much higher for AN composite as compared to the AM composite, because Nb reinforcement is much stronger and ductile as compared to $MoSi_2$ reinforcement. This is reflected in the significant higher flexural strength for AN composite (550 MPa) as compared to AM composite (360 MPa).

5.3. Fracture toughness

A number of toughening mechanisms such as crack deflection [16], microcracking [21], crack blunting [36] and crack bridging [18] have been suggested in literature to explain the toughening in ceramic matrix composites as a result of reinforcement particles. There is, however, an ongoing debate about the relative importance of each of these mechanisms. It is probable that in a given material more than one mechanism acts simultaneously. Although models considering simultaneous and synergistic toughening mechanisms have been developed [37, 38], these models require *a priori* knowledge of the relative contribution of each mechanism involved which is very difficult to determine experimentally.

The observation of crack path - microstructure interactions in AM composite (Fig. 11b) clearly indicates that the primary contribution to toughening in this material originates from crack deflection caused by the $MoSi_2$ particles. The mean deflection angle is $\approx$30°,

which results in only a marginal increase in toughness, as a large deflection angle [$>60^\circ$] is generally required to cause any significant increase in toughness [39]. There is also some evidence of bridging (Fig. 11b), but since $MoSi_2$ itself is brittle at room temperature, the contribution from crack bridging is also insignificant. Single crystals, like SiC whiskers, can remain unfractured due to their inherent high strength and they can bridge the rear of the crack to a significant extent after getting pulled out of the matrix [40]. However, the same is not expected for $MoSi_2$ particles due to their inherent limitations. This is reflected by the marginal increase in toughness in AM composite as compared to unreinforced Al_2O_3.

On the other hand, the microstructure - crack path interaction in the AN composite clearly shows significant crack blunting (Fig. 11c) and bridging because of the Nb particles (Fig. 11d). However, the extent of crack deflection in AN composite is observed to be low. This could be due to lesser propagation of crack path in the material (resulting in lower degree of interaction between crack path and particles) originating from the efficient crack tip blunting mechanism followed by arrest of crack by Nb particles. Nb being ductile, the constrained plastic deformation of Nb particles would require a lot of energy resulting in effective crack tip shielding. This is confirmed by the observation of highly deformed Nb particles on the fractured surface (Fig. 10c). This is also reflected by the three fold increase in fracture toughness in AN composites as compared to monolithic Al_2O_3 matrix. The three fold increase in the present AN composite is comparable to that observed by Waku *et al.* [8] for Al_2O_3 composites reinforced with molybdenum particles of similar size and volume fraction.

It is evident from the present study that addition of Nb particles results in a substantial increase in both flexural strength and fracture toughness at room temperature. On the other hand, the addition of $MoSi_2$ results in only a marginal increase in both flexural strength and fracture toughness. However, at elevated temperature Nb is susceptible to oxidation forming brittle oxides [41], whereas $MoSi_2$ undergoes a brittle to ductile transition phenomenon [42] and the behaviour of these composites could be completely different. High temperature studies are currently underway.

6. Conclusions

1. Dense Al_2O_3 - 25 vol% $MoSi_2$ and Al_2O_3 - 25 vol% Nb composites could be fabricated having uniform distribution of reinforcements throughout the matrix by employing uniaxial vacuum hot pressing route. EPMA results ensured that both $MoSi_2$ and Nb particles had retained their chemical identity in the respective processed composites primarily due to high level of vacuum (10^{-5} torr) achieved during the hot pressing operation.

2. The elastic modulus values of Al_2O_3 / $MoSi_{2p}$ and Al_2O_3 / Nb_p composites were marginally and significantly lower than that of unreinforced Al_2O_3, respectively. The experimentally obtained elastic modulus values for both the composites agree very well with the same calculated theoretically based on modified Tsai - Halpin model.

3. The increase in strength for both the composites in comparison with the monolithic matrix are observed to be primarily due to matrix grain refinement phenomenon and efficient load transfer mechanism to the reinforcement particles. The functioning of load transfer phenomenon can be attributed to the presence of strong and reaction free clean interfaces in both the materials. However, the strength of Al_2O_3 - Nb composite (580 MPa) was observed to be higher than that of Al_2O_3 - $MoSi_2$ material (360 MPa), mainly due to higher load bearing capacity of stronger and ductile Nb particles.

4. Both composites exhibited higher fracture toughness as compared to unreinforced Al_2O_3. The marginal increase in fracture toughness for Al_2O_3 - $MoSi_2$ composite is due to the presence of microscopic crack deflection and crack bridging phenomena. However, the large increase in fracture toughness in Al_2O_3 - Nb composite (3 - fold) could be attributed to crack bridging, significant crack blunting and subsequent arrest by Nb particles.

Acknowledgements

The authors thankfully acknowledge the financial support from the Defence Research and Development Organisation, New Delhi, India. The authors are also grateful to Dr. D. Banerjee, Director, DMRL, Hyderabad, for his suggestions and support extended during the progress of this work.

References

1. M. H. VANDE VOORDE and M. R. NEDELE, *Cer. Engg. & Sci. Proc.* **17** (1996) 3.
2. K. KNOWLES, in Ceram. Technol. Int., 1992, p. 95.
3. K. M. KING, "Advanced Ceramic and Metallic Composites" (University of Cambridge, UK, 1990).
4. K. K. CHAWLA, "Ceramic Matrix Composites" (Chapman & Hall, 1993).
5. B. A. BENDER, D. LEWIS, W. S. COBLENZ and R. W. RICE, *Cer. Engg. & Sci. Proc.* **5** (1984) 513.
6. S.T. OH, T. SEKINO and K. NIIHARA, *ibid.* **18** (1997) 329.
7. T. SEKINO, T. NAKAJIMA and K. NIIHARA, *Mater. Lett.* **29** (1996) 165.
8. Y. WAKU, M. SUZUKI, Y. ODA and Y. KOHTOKU, *Met. and Mater. Trans.* **27A** (1996) 3307.
9. W. B. CHOU and W. H. TUAN, *J. Euro. Cer. Soc.* **15** (1995) 291.
10. D. W. RICHERSON, in "Composite Engineering Handbook," edited by P. K. Mallick (Marcel Dekker Inc., New York, 1997).
11. D. ZHANG, H. YANG, R. YU and W. WENG, *J. Mater. Sci. Lett.* **16** (1997) 877.
12. K. W. CHAE, D. Y. KIM, B. C. KIM and K. B. KIM, *J. Am. Cer. Soc.* **76** (1993) 1857.
13. X. LIN and P. D. OWNBY, *Cer. Engg. & Sci. Proc.* **17** (1996) 273.
14. R. C. GARVIE, *Advances in Ceramics* **12** (1983) 465.
15. N. CLAUSSEN and M. RUHLE, *ibid.* **3** (1981) 137.
16. Y. S. CHOU and D. J. GREEN, *J. Am. Cer. Soc.* **76** (1993) 1985.
17. S. G. SESHADRI, M. SRINIVASAN and K. M. KELLER, *Cer. Engg. & Sci. Proc.* **8** (1987) 671.
18. M. Y. HE, D. J. WISSUCHEK and A. G. EVANS, *Acta Mater.* **45** (1997) 2813.
19. F. D. GAC, *Cer. Engg. & Sci. Proc.* **11** (1990) 551.

20. C. C. WU, S. W. FREIMAN, R. W. RICE and J. J. MECHOLSKY, *J. Mater. Sci.* **13** (1978) 2659.
21. A. G. EVANS and K. T. FABER, *J. Am. Cer. Soc.* **64** (1981) 394.
22. J. J. PETROVIC, *MRS Bulletin* **18** (1993) 35.
23. J. J. PETROVIC and A. K. VASUDEVAN, in Mat. Res. Soc. Symp. Proc. (Materials Research Society, 1994) Vol. 322, p. 3.
24. J. J. PETROVIC and R. E. HONNELL, *J. Mater. Sci. Lett.* **9** (1990) 1083.
25. M. P. BOROM, M. K. BRUN and L. E. SZALA, *Cer. Engg. & Sci. Proc.* **8** (1987) 654.
26. D. KNAUSS and W. MADER, *Ultramicroscopy* **37** (1991) 247.
27. A. K. VASUDEVAN and J. J. PETROVIC, *Mater. Sci. & Engg.* **A155** (1992) 1.
28. A. G. EVANS and B. J. DALGLEISH, *ibid.* **A162** (1993) 1.
29. Y. S. CHOU and D. J. GREEN, *J. Am. Cer. Soc.* **76** (1993) 1452.
30. Annual Book of ASTM Standards, ASTM Standard E 399 - 83, Section 3, Philadelphia, PA, USA, 1990, p. 500.
31. K. K. CHAWLA, in "Composite Materials: Science and Engineering," edited by B. Ilschner and N. J. Grant (Springer - Verlag, New York, 1987) p. 177.
32. H. LAGACE and D. J. LLOYDS, *Canadian Met. Quart.* **28** (1989) 145.
33. Z. HASHIN and S. SHTRIKMAN, *J. Mech. Phys. Solids* **2** (1973) 126.
34. S. GERARDI, "Metals Handbook, Vol. 2: Niobium," 10th ed. (ASM International, The Materials Information Society, 1990) p. 565.
35. R. WARREN, "Ceramic Matrix Composites" (Chapman & Hall, New York, 1992) p. 2.
36. K. S. CHAN, *Met. Trans.* **23A** (1992) 183.
37. A. A. MORRONE, S. R. NUTT and S. SURESH, *J. Mater. Sci.* **23** (1988) 3206.
38. J. RODEL, E. R. FULLER JR. and B. R. LAWN, *J. Am. Cer. Soc.* **74** (1991) 3154.
39. S. SURESH, *Met. Trans.* **16A** (1985) 249.
40. P. F. BECHER, *J. Am. Cer. Soc.* **74** (1991) 255.
41. M. RUHLE, M. BACKHAUS - RICOULT, K. BURGER and W. MADER, in Proceedings of the Conference on "Ceramic Microstructures '86 : The Role of Interfaces," edited by J. A. Pask and A. G. Evans (Univ. of California Press, Berkeley, USA, 1986) p. 295.
42. R. M. AIKIN JR., *Scripta Met. Mater.* **26** (1992) 1025.

Received 15 June 1999
and accepted 3 February 2000